OPEN

ORIGINAL ARTICLE

Adding fifth dimension to optoacoustic imaging: volumetric time-resolved spectrally enriched tomography

Xosé Luís Deán-Ben and Daniel Razansky

Optoacoustics provides a unique set of capabilities for bioimaging, associated with the intrinsic combination of ultrasound- and light-related advantages, such as high spatial and temporal resolution as well as powerful spectrally enriched imaging contrast in biological tissues. We demonstrate here, for the first time, the acquisition, processing and visualization of five-dimensional optoacoustic data, thus offering unparallel imaging capacities among the current bioimaging modalities. The newly discovered performance is enabled by simultaneous volumetric detection and processing of multispectral data and is further showcased here by attaining time-resolved volumetric blood oxygenation maps in deep human vessels and real-time tracking of contrast agent distribution in a murine model *in vivo*.

INTRODUCTION

More than a century ago, A G Bell and C S Tainter first detected sound waves generated by an intensity modulated beam of sunlight.[1] Measurement of ultrasonic waves, induced by absorption of short-pulsed light in tissue chromophores, is also the basic principle behind modern optoacoustic imaging.[2] Yet, despite the ancient discovery of the basic physical phenomenon, it was not until very recently that optoacoustics was first applied to biomedical imaging, experiencing an exponential growth of technical developments and related applications in the last decade.[3–6] Being a time-resolved signal, a single optoacoustic waveform may provide one-dimensional depth profiling information, similarly to A-mode visualizations in ultrasound imaging.[7] Thereby, the simplest way of acquiring two- or three-dimensional (3D) optoacoustic images consists of using linear raster scanning of a spherically focused ultrasonic transducer along the surface of the imaged object and stacking up sets of the measured signals, a method utilized by most existing optoacoustic microscopy set-ups.[4,8–10]

However, scanning imaging systems are generally afflicted with long acquisition times, while focused detection inevitably results in out-of-focus artifacts, leading to lack of quantification and overall reduced image quality.[11] Alternatively, optoacoustic tomographic systems have been suggested, based on simultaneous acquisition of optoacoustically induced signals at multiple locations surrounding the imaged object.[12] One recent approach utilized parallel detection of optoacoustic signals with an array of cylindrically focused ultrasonic transducers in order to generate high-resolution cross-sectional images at video rate.[13] The real-time performance has dramatically reduced image artifacts associated with motion, such as heart beat and breathing.

Furthermore, visualization of dynamic processes, including hemodynamic changes, imaging of kinetics and real-time biodistribution of contrast agents, has become possible.[14,15] Yet, in this way, volumetric imaging can only be achieved by scanning the detection array along the imaged object, while the overall quasi-two-dimensional approach introduces significant challenges associated with out-of-plane signals.[16] More recently, feasibility of four-dimensional imaging, i.e., 3D imaging in real time, was also showcased with a system based on simultaneous unfocused detection of signals at multiple locations densely distributed on a spherical surface.[17,18]

In all cases, the time resolution of the imaging method is limited by the pulse repetition rate of the laser employed and is further reduced if acquisition of data at multiple wavelengths is done, thus eliminating the possibility of real-time imaging due to the time lapse for wavelength tuning. Multispectral imaging, however, presents important advantages in efficient visualization of spectrally distinct tissue chromophores as well as extrinsically administered biomarkers in the presence of highly absorbing background. By imaging at different optical wavelengths, multispectral optoacoustic tomography provides spectral specificity using an additional (wavelength) dimension. As a large variety of substances present a characteristic absorption spectrum in the visible and near infrared, multispectral optoacoustic tomography provides a versatile way of interrogation and visualization of functional and molecular processes in living tissues, with multiple applications in small animal research continuously emerging,[19] while promising prospects for clinical applications are further envisioned.[6,20] An alternative approach to obtain multispectral information in real time consists in simultaneously collecting the signals generated by two laser pulses shifted in time by the order of microseconds.[21,22]
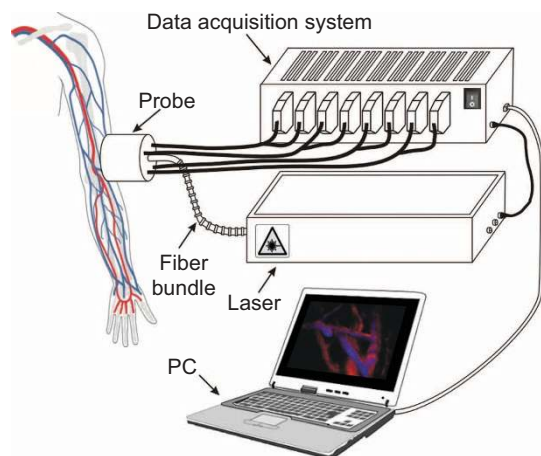
Institute for Biological and Medical Imaging (IBMI), Technical University of Munich and Helmholtz Center Munich, 85764 Neuherberg, Germany
Correspondence: Dr D Razansky, Institute for Biological and Medical Imaging (IBMI), Technical University of Munich and Helmholtz Center Munich, Ingolstädter Landstraβe 1, 85764 Neuherberg, Germany
E-mail: dr@tum.de

Figure 1 Schematics and the clinical hand-held optoacoustic imaging scanner. Optical illumination is provided with a fiber bundle guiding the ouptut beam of the laser. The optoacoustic probe is acoustically matched to the imaged tissue by means of a transparent membrane containing a coupling fluid (water). A 1-Gbit ethernet connection is used to transmit the optoacoustic signals collected with the data acquisition system to a personal computer, where GPU-based data processing is performed to attain real-time visualization. GPU, graphics processing unit.

However, biological tissues always contain multiple (more than two) spectrally distinct chromophores, thus, in general, more than two optical wavelengths are necessary to perform efficient spectral unmixing of the different absorbing substances.

Here we overcome the existing limitations by designing a novel optoacoustic imaging system that is able to acquire, process and visualize five-dimensional (5D) optoacoustic data, i.e., deliver volumetric spectrally enriched tomography in real time, offering an unparallel imaging performance among the current bioimaging modalities. This is achieved by using a newly developed high pulse repetition rate laser with fast wavelength tuning capabilities, combined with simultaneous detection of 3D optoacoustic data over a spherical surface surrounding the object.

MATERIALS AND METHODS

Experimental set-up

The experimental system is depicted in Figure 1. It consists of a laser light source, custom-made spherical array ultrasonic probe[23], parallel acquisition system and a computer. The illumination source is a custom-made optical parametric oscillator-based laser, generating 5 ns duration pulses with energy of up to 20 mJ at a pulse repetition rate of up to 50 Hz (Innolas Laser GmbH, Krailling, Germany). A dedicated tuning system based on fast mechanical rotation of the optical parametric oscillator crystal has been developed that allows changing the wavelength to any value between 700 and 900 nm on a per-pulse basis. In this way, it only takes 100 ms to acquire an entire volumetric multispectral dataset at five different wavelengths. The light beam is guided through a custom-made fiber bundle (CeramOptec GmbH, Bonn, Germany) toward the imaged object. The bundle is terminated in the center of the spherical detection surface and the beam reaches the surface of the object with a spot size of approximately 1 cm. The optoacoustically generated volumetric data are collected by the matrix array consisting of 256 adjacent piezoelectric elements with a size of approximately 3×3 mm^2 densely placed on the spherical

surface, which covers a solid angle of 90°. This configuration, having relatively large and densely packed detection elements, further ensures optimal signal-to-noise ratio performance and ability to collect high quality volumetric data for each illumination pulse without signal averaging. Furthermore, all elements are conveniently oriented towards the center of the sphere in order to provide good sensitivity in the imaged region of interest. The detection elements are centered around 4 MHz and have an available bandwidth of about 100%, which corresponds to a spatial resolution of approximately 200 μm in the center of the imaged region (geometrical center of the sphere). The pressure signals, received by all the elements, are simultaneously sampled at 2030 instants with a sampling frequency of 40 megasamples per second. This is done by a custom-made data acquisition system (Falkenstein Mikrosysteme GmbH, Taufkirchen, Germany) consisting of 256 parallel analog to digital converters arranged in eight acquisition cards, simultaneously processing 32 channels each. This provides simultaneous acquisition of the optoacoustic signals at the pulse repetition rate of the laser and their subsequent transmission to a personal computer through a 1 Gbit ethernet connection. The spherical ultrasonic array is matched to the imaged object using a transparent membrane, whereas the space between the membrane and the detection surface is filled with a matching fluid (water). Its transparency also guarantees efficient illumination of the object through the fiber bundle without energy loss.

Image reconstruction methods

On-the-fly reconstruction and visualization of single-wavelength 3D images is enabled by graphics processing unit-based processing. Prior to image reconstruction, the acquired signals are deconvolved with the electrical impulse response of the array elements and band-pass filtered with cutoff frequencies between 0.1 and 5 MHz. The size of the reconstructed 3D region of interest was set to $15 \times 15 \times 7$ mm^3 ($150 \times 150 \times 70$ voxels). From the multiple volumetric images retrieved at the measured wavelengths, distribution maps of different chromophores were subsequently retrieved by utilizing an unmixing procedure that consisted of least-square fitting the reconstructed optical absorption to the molar extinction coefficients of the tissue chromophores (Figure 2a). The unmixing procedure has been previously described.[3] Real-time image visualization during data acquisition is enabled by our current graphics processing unit implementation, which is able to perform 3D backprojection reconstruction and spectral unmixing in less than 20 ms. Nevertheless, for best quantitative performance in processing of the multispectral data, optoacoustic image reconstruction for the spectrally unmixed images presented here was instead performed offline with a 3D model-based inversion algorithm.[24]

In vivo human imaging

Human imaging experiments were done in full accordance with work safety regulations of Helmholtz Center Munich. The pulse repetition rate of the laser and the per-pulse energy are selected in a way so that laser safety standards for clinical measurements are fulfilled at all times.[25] The *in vivo* experiments were conducted in the wrist region of a healthy volunteer. Prior to the experiments, hair was removed around the imaged region in order to avoid image artifacts due to strong optoacoustic signals from the skin surface. During imaging, the hand-held probe was gently moved along the skin surface with an average speed of approximately 2 mm s^{-1} while acquiring the multispectral volumetric data.
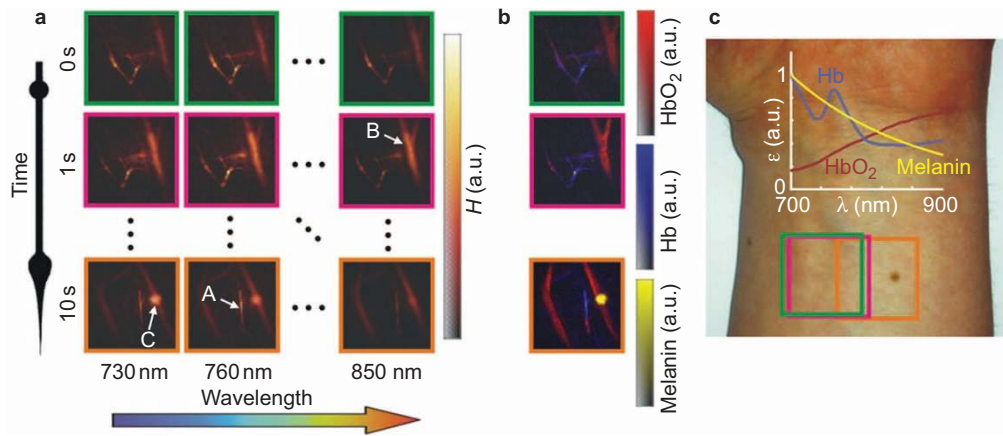
Figure 2 Demonstration of five-dimensional optoacoustic imaging in a healthy volunteer *in vivo* using the hand-held probe. (**a**) Two-dimensional matrix of reconstructed volumetric optoacoustic images (maximal intensity projection along the depth direction is shown). Each image corresponds to data taken at a different wavelength and a different time point, thus, effectively rendering five-dimensional data set. (**b**) For each time point, the wavelength-dependent data are unmixed in order to render, in real time, distribution maps of three different intrinsic tissue chromophores. (**c**) Photograph from a human forearm, from which the images were taken. Spectral dependence of the optical absorption of the three main tissue chromophores is also shown. The colored frames correspond to the region of interest from which the data were acquired for each of the three time points shown in (**a**).

In vivo mouse imaging

Procedures involving animals and their care were conducted in conformity with institutional guidelines and with approval from the Government of Upper Bavaria. Eight-week-old female nude CD-1 mice were anaesthetized with 2% isoflurane throughout the experiments. The head of the mouse was arranged on top of the hand-held probe in a supine position (Figure 3a). Brain vasculature of the mouse was tracked over 36 s starting 5 s before injection of the indocyanine green (ICG) contrast agent (PULSION Medical Systems SE, Feldkirchen, Germany). This particular agent was selected for demonstration purposes due to its well-studied fluorescence and optoacoustic properties. It is an FDA-approved, water-soluble, inert anionic tricarbocyanine dye that has been established as a tool to investigate a variety of different clinical endpoints. For the 5D *in vivo* imaging study of ICG kinetics, 10 nmol or 50 nmol of ICG was injected i.v. diluted in 50 μL of saline.

RESULTS

In vivo human imaging has been subsequently demonstrated in a healthy volunteer. The pulsed laser fluence on the skin surface was kept below the exposure safety limits of 20 mJ cm^{-2} for the entire duration of the experiments.[25] The measurements were done in the wrist region, having large variety of vasculature of different sizes, depth and oxygenation levels, as well as a melanin-rich skin pigmentation, which presents characteristic spectral variations in addition to oxygenated and deoxygenated hemoglobin. The absorption spectra of the different tissue chromophores are displayed in Figure 2c in arbitrary units. The 5D optoacoustic imaging experiments were done by real-time acquisition of volumetric datasets at multiple wavelengths between 730 and 850 nm, corresponding to a monotonic decrease in the absorption of melanin, a monotonic increase in the absorption of oxygenated hemoglobin and a characteristic peak in the absorption of deoxygenated hemoglobin. It was further assumed that tissue absorption is mainly due to the above mentioned three dominant chromophores. Measurements were performed by scanning the hand-held probe along the skin surface.

Experimental results are presented in Figure 2a. The matrix of images corresponds to the 5D data set, i.e., each volumetric image was acquired at a different wavelength and time instant during the experiment. Fast wavelength tuning ensured that no significant motion occurred during acquisition of the multiwavelength datasets at a certain location of the hand-held probe. The characteristic spectral variations of different vessels can be readily perceived in the single-wavelength images. For instance, the optical absorption in the vessel marked 'A' in Figure 2a presents a peak at 760 nm and decreases for longer wavelengths, which indicates presence of deoxygenated hemoglobin. On the other hand, the optical absorption in the vessel marked 'B' in Figure 2b monotonically increases with wavelength, representing characteristic spectral behavior of oxygenated hemoglobin. A strongly absorbing skin pigmentation can be further identified in the central part of the images acquired at the $t=10$ s time point (marked 'C' in Figure 2a), indicating a clearly decreasing absorption with wavelength due to its high melanin content. The unmixed images, representing distribution of the individual tissue chromophores at three distinct time points, are further shown in Figure 2b. Finally, the entire series of multispectral optoacoustic images, acquired during manual scanning of the probe, is available as Supplemetary Movie 1. Despite the fast wavelength tuning capability of the laser, which was designed to overcome image artifacts associated with motion between images acquired at different wavelengths, certain motion artifacts were still present in small number of image frames, mainly due to irregular movements of the hand-held probe manually scanned by the user. Frames containing motion artifacts were eliminated in post processing by correlating images acquired at different wavelengths.

Figure 3 shows results of an *in vivo* mouse brain imaging experiment that monitored an intravenous injection of ICG. As described in detail in the section on 'Materials and methods', the ultrasound array remained in a fixed position throughout the measurement, while the head of the anesthetized mouse was placed on top of the hand-held probe in a supine position (Figure 3a). The ICG contrast agent was tracked over 36 s during injection. Figure 3b shows typical maximum intensity projection images of the brain vasculature before (baseline) and after injection of two different concentrations of ICG at a wavelength of 800 nm, corresponding to the peak absorption of the probe. The contrast agent can be readily identified in the single wavelength images when a relatively high amount (50 nmol) of the probe is injected into the mouse. However, this is certainly not the case
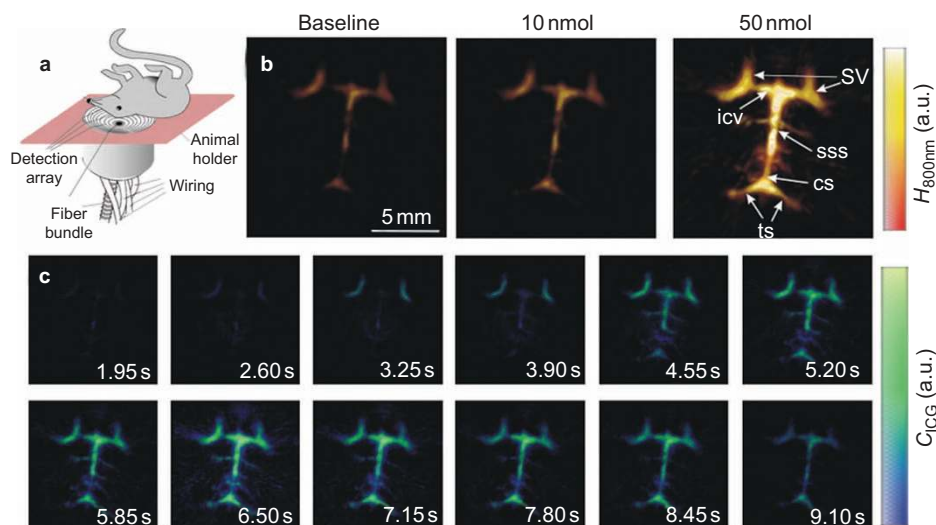
Figure 3 Five-dimensional imaging of mouse brain perfusion *in vivo*. (**a**) Layout of the experimental set-up. (**b**) Single-wavelength images (maximal intensity projection along the depth direction) acquired before and after injection of the ICG contrast agent. Results for two different concentrations are shown. When 10 nmol of ICG was injected, the contrast agent cannot be easily distinguished from the background blood absorption. Different structures in the mouse brain are indicated in the figure, supraorbital veins (sv), inferior cerebral vein (icv), superior sagital sinus (sss), confluence of sinuses (cs) and transverse sinus (ts). (**c**) Time series of images after spectral unmixing of multiwavelength data, taken for the 10 nmol experiment, clearly reveals the inflow of the agent *in vivo* and in real time. ICG, indocyanine green.

when a more realistic amount of only 10 nmol is injected, in which case the agent is not easily distinguishable due to its relatively low concentration in the highly absorbing blood background. In contrast, spectral processing of the real-time multiwavelength data clearly reveals biodistribution of the agent in real time, as shown in Figure 3c. The actual performance can be best appreciated in Supplementary Movie 2, showing rotational 3D movie of the brain vasculature as the agent distributes through it.

As compared to the experiment presented in Figure 2, the latter experiment demonstrates a different application of 5D optoacoustic data for visualization of dynamic events *in vivo*. While for the human wrist imaging, the biological data remained stationary with the hand-held probe moved in order to visualize different parts of the body, the mouse experiments have demonstrated the capability of acquiring dynamic multispectral biological data in real time as the contrast agent was distributing through the brain vasculature.

The current work represents a significant improvement in the sensitivity of optoacoustic tomography for deep tissue imaging applications as previous whole-body mouse imaging implementations have employed much higher dye concentrations of 40 nmol and more in systemic *in vivo* injections.[13,14] We believe that this could be partially attributed to the more quantitative nature of the present 3D imaging configuration versus quasi-two-dimensional data collection systems that introduce significant inaccuracies and artifacts associated with out-of-plane signals.[16] Yet, the achievable sensitivity in deep tissue multispectral optoacoustic imaging depends on multiple additional factors, such as the signal-to-noise ratio of the acquired signals, per-pulse energy oscillations, wavelength-dependent light attenuation or the unmixing algorithm employed.[19,26,27] The quantification issue is on its own a complicated and long-standing challenge[28] that deserves a separate attention. Generally, the amplitude of optoacoustic signals is a nonlinear product of the non-uniform light fluence in tissue, the heterogenous optical absorption coefficient and the tissue-dependent Grüneisen parameter.[29] The absorption coefficient itself is proportional to the added contribution of absorption by different chromophores, each represented by a product of its molar extinction

coefficient and concentration. In order to provide quantitative values of the concentration of different chromophores, one must also account for the strong (and generally unknown) wavelength-dependent light fluence distribution[29] and the spatial distribution of the Grüneisen parameter,[30] as well as acoustic heterogeneities[31–33] and attenuation[34] in the object. Furthermore, a correct calibration of the space- and frequency-dependent sensitivity of the ultrasonic transducers[35,36] is needed to relate the collected voltage to the actual optoacoustic pressure. Even though in the current work we were clearly able to attain reasonable qualitative values regarding relative concentration of the different tissue chromophores and dynamics of the dye biodistribution, we are still restrained from claiming absolute quantification for imaging at a centimeter-scale depth. This topic would indeed require intensive investigations in the years to come.

CONCLUSIONS

In summary, the results presented herein demonstrate, for the first time to our knowledge, the feasibility of optoacoustic imaging in five dimensions, i.e., rendering volumetric images of spectrally resolved optoacoustic data in real time. These never-seen-before capacities of the optoacoustic technology open new prospects with several important applications envisioned in clinical practice as well as in preclinical research. The convenience of the hand-held operation, combined with the real-time visualization performance in 3D, makes our system ideal for studying functional blood parameters in a real clinical setting, e.g., for diagnostic purposes of peripheral vasculature disease, breast lesions, lymph nodes and other indications. The ability to track biodistribution of specific substances in real time and in the entire volume of interest may further open new possibilities in small animal imaging applications, e.g., *in vivo* cell tracking, visualization of pharmacokinetics, targeted molecular imaging studies and neuroimaging. Finally, the spectral unmixing capabilities can be used in order to simultaneously visualize several spectrally distinct endogenous chromophores and extrinsically administered contrast agents. Clearly, visualization of higher number of targets would require increasing the number of scanned wavelengths, which would slow down the imaging frame rate.

Our future work will therefore concentrate on increasing wavelength tuning speed to enable faster frame rates as well as addressing other important algorithmic challenges, such as quantification and sensitivity of spectrally unmixed images.

ACKNOWLEDGMENTS

1 Tainter CS, Bell AG. Selenium and the photophone. *Nature* 1880; **22**: 500–503.
2 Wang LV. *Photoacoustic Imaging and Spectroscopy*. Boca Raton, FL: CRC Press; 2009.
3 Razansky D, Distel M, Vinegoni C, Ma R, Perrimon N *et al*. Multispectral opto-acoustic tomography of deep-seated fluorescent proteins *in vivo*. *Nat Photon* 2009; **3**: 412–417.
4 Wang LV. Multiscale photoacoustic microscopy and computed tomography. *Nat Photon* 2009; **3**: 503–509.
5 de la Zerda A, Zavaleta C, Keren S, Vaithilingam S, Bodapati S *et al*. Carbon nanotubes as photoacoustic molecular imaging agents in living mice. *Nat Nanotechnol* 2008; **3**: 557–562.
6 Yang JM, Favazza C, Chen R, Yao J, Cai X *et al*. Simultaneous functional photoacoustic and ultrasonic endoscopy of internal organs *in vivo*. *Nat Med* 2012; **18**: 1297–1302.
7 Kim JW, Galanzha EI, Shashkov EV, Moon HM, Zharov VP. Golden carbon nanotubes as multimodal photoacoustic and photothermal high-contrast molecular agents. *Nat Nanotechnol* 2009; **4**: 688–694.
8 Ma R, Sontges S, Shoham S, Ntziachristos V, Razansky D. Fast scanning coaxial optoacoustic microscopy. *Biomed Opt Express* 2012; **3**: 1724–1731.
9 Zhang HF, Maslov K, Stoica G, Wang LH. Functional photoacoustic microscopy for high-resolution and noninvasive *in vivo* imaging. *Nat Biotechnol* 2006; **24**: 848–851.
10 Yao JJ, Maslov KI, Zhang Y, Xia YN, Wang LV. Label-free oxygen-metabolic photoacoustic microscopy *in vivo*. *J Biomed Opt* 2011; **16**: 076003.
11 Beard P. Biomedical photoacoustic imaging. *Interface Focus* 2011; **1**: 602–631.
12 Brecht HP, Su R, Fronheiser M, Ermilov SA, Conjusteau A *et al*. Whole-body three-dimensional optoacoustic tomography system for small animals. *J Biomed Opt* 2009; **14**: 064007.
13 Razansky D, Buehler A, Ntziachristos V. Volumetric real-time multispectral optoacoustic tomography of biomarkers. *Nat Protoc* 2011; **6**: 1121–1129.
14 Taruttis A, Morscher S, Burton NC, Razansky D, Ntziachristos V. Fast multispectral optoacoustic tomography (MSOT) for dynamic imaging of pharmacokinetics and biodistribution in multiple organs. *PLoS ONE* 2012; **7**: e30491.
15 Buehler A, Herzog E, Ale A, Smith BD, Ntziachristos V *et al*. High resolution tumor targeting in living mice by means of multispectral optoacoustic tomography. *EJNMMI Res* 2012; **2**: 14.
16 Queiros D, Dean-Ben XL, Buehler A, Razansky D, Rosenthal A *et al*. Modeling the shape of cylindrically focused transducers in three-dimensional optoacoustic tomography. *J Biomed Opt* 2013; **18**: 76014.
17 Buehler A, Dean-Ben XL, Claussen J, Ntziachristos V, Razansky D. Three-dimensional optoacoustic tomography at video rate. *Opt Express* 2012; **20**: 22712–22719.
18 Xiang LZ, Wang B, Ji LJ, Jiang HB. 4-D photoacoustic tomography. *Sci Rep* 2013; **3**: 1113.
19 Ntziachristos V, Razansky D. Molecular imaging by means of multispectral optoacoustic tomography (MSOT). *Chem Rev* 2010; **110**: 2783–2794.
20 Heijblom M, Piras D, Xia W, van Hespen JC, Klaase JM *et al*. Visualizing breast cancer using the Twente photoacoustic mammoscope: what do we learn from twelve new patient measurements? *Opt Express* 2012; **20**: 11582–11597.
21 Galanzha EI, Shashkov EV, Kelly T, Kim JW, Yang LL *et al*. *In vivo* magnetic enrichment and multiplex photoacoustic detection of circulating tumour cells. *Nat Nanotechnol* 2009; **4**: 855–860.
22 Wang LD, Maslov LH. Single-cell label-free photoacoustic flowoxigraphy *in vivo*. *Proc Natl Acad Sci USA* 2013; **110**: 5759–5764.
23 Deán-Ben XL, Razansky D. Portable spherical array probe for volumetric realtime optoacoustic imaging at centimetre-scale depths. *Opt Express* 2013; **21**: 28062–28071.
24 Dean-Ben XL, Buehler A, Ntziachristos V, Razansky D. Accurate model-based reconstruction algorithm for three-dimensional optoacoustic tomography. *IEEE Trans Med Imaging* 2012; **31**: 1922–1928.
25 *American National Standards for the Safe Use of Lasers ANSI Z136.1*. Orlando, FL: American Laser Institute; 2000.
26 Razansky D, Baeten J, Ntziachristos V. Sensitivity of molecular target detection by multispectral optoacoustic tomography (MSOT). *Med Phys* 2009; **36**: 939–945.
27 Kim C, Favazza C, Wang LH. *In vivo* photoacoustic tomography of chemicals: high-resolution functional and molecular optical imaging at new depths. *Chem Rev* 2010; **110**: 2756–2782.
28 Lutzweiler C, Razansky D. Optoacoustic imaging and tomography: reconstruction approaches and outstanding challenges in image performance and quantification. *Sensors* 2013; **13**: 7345–7384.
29 Cox B, Laufer JG, Arridge SR, Beard PC. Quantitative spectroscopic photoacoustic imaging: a review. *J Biomed Opt* 2012; **17**: 061202.
30 Wang LV. Tutorial on photoacoustic microscopy and computed tomography. *IEEE J Sel Top Quant* 2008; **14**: 171–179.
31 Jose J, Willemink RG, Steenbergen W, Slump CH, van Leeuwen TG *et al*. Speed-of-sound compensated photoacoustic tomography for accurate imaging. *Med Phys* 2012; **39**: 7262–7271.
32 Huang C, Wang K, Nie LM, Wang LH, Anastasio MA. Full-wave iterative image reconstruction in photoacoustic tomography with acoustically inhomogeneous media. *IEEE Trans Med Imaging* 2013; **32**: 1097–1110.
33 Dean-Ben XL, Ntziachristos V, Razansky D. Artefact reduction in optoacoustic tomographic imaging by estimating the distribution of acoustic scatterers. *J Biomed Opt* 2012; **17**: 110504.
34 Dean-Ben XL, Razansky D, Ntziachristos V. The effects of acoustic attenuation in optoacoustic signals. *Phys Med Biol* 2011; **56**: 6129–6148.
35 Wang K, Ermilov SA, Su R, Brecht HP, Oraevsky AA *et al*. An imaging model incorporating ultrasonic transducer properties for three-dimensional optoacoustic tomography. *IEEE Trans Med Imaging* 2011; **30**: 203–214.
36 Caballero MA, Rosenthal A, Buehler A, Razansky D, Ntziachristos V. Optoacoustic determination of spatio-temporal responses of ultrasound sensors. *IEEE Trans Ultrason Ferroelectr Freq Control* 2013; **60**: 1234–1244.

Supplementary Information for this article can be found on *Light: Science & Applications*' website (http://www.nature.com/lsa/).